Modeling and Inverse Compensation of Hysteresis in Supercoiled Polymer Artificial Muscles

Jun Zhang, Kaushik Iyer, Anthony Simeonov, and Michael C. Yip, *Member, IEEE*

***Abstract*—The supercoiled polymer (SCP) actuator is a recently discovered artificial muscle that demonstrates significant mechanical power, large contraction, and good dynamic range in a muscle-like form factor. There has been a rapid increase of research efforts devoted to the study of SCP actuators. For robotics, SCP actuators overcome specific challenges of artificial muscles such as shape memory alloy wires, where limited strain and slow dynamics, and power consumption had limited their use. It is known that hysteresis nonlinearity results from coiling the threads, and can cause up to 30% strain difference under the same voltage; however, no work has been reported to characterize the hysteresis in SCP actuators. In this paper, three new models are formulated to characterize the hysteretic relationship between three coupled variables (voltage input, strain, and load) of an SCP actuator, namely, the augmented generalized Prandtl–Ishlinskii model, the augmented Preisach model, and the augmented linear model. By incorporating the relationship between hysteresis curves and loading forces, the proposed models can efficiently characterize the hysteresis. Open-loop position control is further realized through inverse compensation. Experimental results show that the proposed schemes can effectively estimate and compensate the hysteresis. For the first time, the hysteresis characterization and compensation of SCP actuators are successfully demonstrated, such that accurate robot control can be realized.**

***Index Terms*—Hydraulic/pneumatic actuators, novel actuators for natural machine motion.**

I. Introduction

As a recently discovered artificial muscle, the super-coiled polymer (SCP) actuators demonstrate significant mechanical power, large contraction, and good dynamic range in a muscle-like form factor [1]. Originally, SCP actuators were produced by twisting carbon nanotube (CNT) yarns until coils were formed and were capable of being activated electrically, chemically, and photonically [2]. It was recently showed that the similar effect can be obtained using commercially available nylon fishing lines and sewing threads by Joule heating [3], as shown in Fig. 1(a)–(c). Up to 20% tensile actuations (strain) were demonstrated with the non-mandrel-coiled SCP actuators. The mandrel-coiled ones can generate up to 50% strain [3]. Our recent work [4] demonstrated that the relaxation time of SCP actuators was on the order of 1s. SCP actuators produce significantly larger strain and have faster relaxation speed, compared to shape memory alloy (SMA) wires, which only produce 4-5% strain and the relaxation time often results in an order of 10 s [5], [6]. Despite being a recent discovery, SCP actuators show strong promise of being a transformative artificial muscle technology for robotics and mechatronic systems in general.

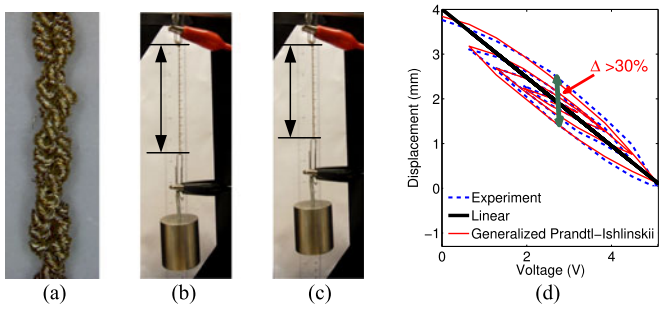

Fig. 1. (a) A super-coiled polymer (SCP) muscle constructed from coiling a nylon thread (V Technical Textiles, 110/34 dtex). One SCP actuator at (b) room temperature (uncontracted), and at (c) high temperature (contracted). 15% contraction is observed. (d) Comparison between a generalized Prandtl-Ishlinskii (GPI) model and a linear model for capturing the hysteresis between displacement and voltage of an SCP actuator under 30 g loading.

There has been a rapid increase of research efforts devoted to fabrication, characterization and application of SCP actuators. By coating nylon fishing line with conductive silver paint, Joule heating can be utilized to control the SCP actuators [7]. The mechanical behavior of SCP actuators was characterized by testing the elastic modulus and tensile stroke over a wide range of temperature values and loads [8]. The thermoelectric properties of SCP actuators were described and compared under still air, forced air, and water environments [4]. Various applications utilizing SCP actuators have been recently developed. In our paper [4], we demonstrated the first robotic hand and arm with SCP actuation. In [9], a biomimetic structure of SCP actuators imitating the human pennate muscle was presented, and the ability to change stiffness was demonstrated. SCP actuators were utilized for driving robotic fingers in [4], [10], [11]. The design of a wearable wrist orthosis incorporated with SCP actuators was demonstrated in [12], showing promise in rehabilitation therapy and human assistance.

Manuscript received September 10, 2016; revised November 29, 2016; accepted December 21, 2016. Date of publication January 11, 2017; date of current version February 2, 2017. This paper was recommended for publication by Associate Editor J. Ueda and Editor P. Rocco upon evaluation of the reviewers comments.

J. Zhang and M. C. Yip are with the Department of Electrical and Computer Engineering, University of California, San Diego, La Jolla, CA 92093 USA (e-mail: j5zhang@ucsd.edu; yip@ucsd.edu).

K. Iyer is with the Department of Bioengineering, University of California, San Diego, La Jolla, CA 92093 USA (e-mail: kiyer@ucsd.edu).

A. Simeonov is with the Department of Mechanical and Aerospace Engineering, University of California, San Diego, La Jolla, CA 92093 USA (e-mail: asimeono@ucsd.edu).

Color versions of one or more of the figures in this letter are available online at http://ieeexplore.ieee.org.

Digital Object Identifier 10.1109/LRA.2017.2651401

With the significant interest in SCP actuators among the robotics community, however, limited work has been conducted to study the modeling and control of these actuators. Coiling and twisting of fiber threads was suggested to introduce friction and nonlinear hysteretic effects [1]. Prior studies have reported the hysteretic relationships between force and strain [4], [9], and strain and temperature [3] in SCP actuators, but no work has been available on characterizing and compensating the hysteresis. As shown in Fig. 1(d), the linear model fails to capture the hysteresis and could produce over 15% modeling error. Our preliminary work [4] is the first to model and control SCP actuators, but hysteresis was not considered in the analysis. Force and position control were realized [12]–[14], but only linear models and controls were adopted. The existing methods accounted for hysteresis in a damping term that only provided a modest approximation of hysteresis, and only for dynamic behavior, but cannot describe the static hysteretic effects. Thus, control deficiencies existed, especially in open-loop control.

Modeling and control of systems with hysteresis has been an active research area, especially for various smart materials-based systems. While physics-based models [15] only work for particular materials, phenomenological models present a more generalizable solution and are more widely adopted [16]–[29]. Prandtl-Ishlinskii (PI) model [16]–[22] and Preisach model [23]–[26] are among the most popular hysteresis models, and have both proven to be effective. The PI model consists of a weighted superposition of play operators and has lower computational cost compared with the Preisach model [22]. While the classical PI (CPI) model [17] only works for symmetric hysteresis, the generalized PI (GPI) model [18], [21], [22] can capture asymmetric hysteresis. Existing studies often adopt a single hysteresis model to capture a particular hysteretic relationship [18], [19], [24]. However, the hysteresis curves in SCP actuators between voltage input and contraction length are different under different loading forces, which further complicates the modeling. A predominant class of control strategies for hysteretic systems involves approximate cancellation of the hysteresis through inverse compensation [17]–[19], [24], [25], [30]–[32]. While the realization of the Preisach model inverse involves numerical iteration [24], [25], the GPI model has an analytical inverse [18] for efficient implementation.

This paper presents the *first* study on the modeling and inverse compensation of hysteresis in SCP actuators. Three new models are formulated to characterize a series of hysteresis curves between voltage input and contraction length of an SCP actuator under different loading forces, namely, the augmented GPI model, the augmented Preisach model, and the augmented linear model. By incorporating the relationship between hysteresis curves and loading forces, the proposed models can efficiently characterize and estimate the hysteresis in SCP actuators. Open-loop position control is further realized through inverse compensation. Experimental results show that the proposed schemes can effectively estimate and compensate the hysteresis. The modeling and control accuracy as well as the computational efficiency of the three approaches are compared. For example, the maximum modeling errors are 7.5%, 7.3%, and 20.4%, under the augmented GPI, Preisach, and linear models, respectively.

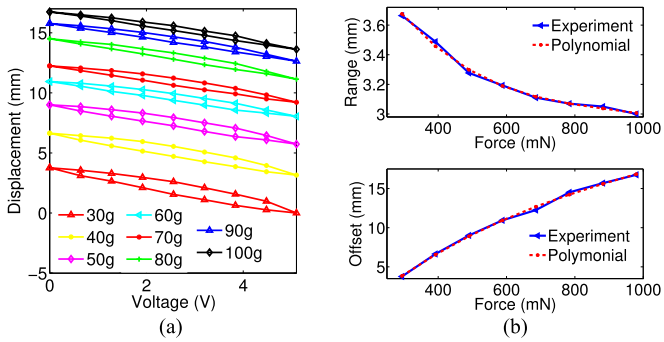

Fig. 2. (a) The hysteresis between voltage and displacement of an SCP actuator under different loading forces. (b) Displacement ranges (upper figure) and initial displacements (lower figure) under different loading forces. Note how the force, voltage and displacements are coupled, a challenge for realizing robot control.

The contributions of this work are: (1) hysteresis modeling for SCP actuators using augmented versions of three popular hysteresis modeling methods, (2) inverse compensation of SCP actuators for open-loop position control, (3) experimental validation of modeling and inverse compensation.

II. Characterization and Discussion

A. Characterization

Heating the SCP actuator causes significant contraction, which can be explained as follows. Before coiling, the polymer chains within the thread are parallel. These polymer chains are twisted into helices when the thread is coiled. When the coiled thread is heated, both length contraction of the polymer chains and thread diameter expansion cause thread untwist. The produced torque of untwisting induces the contraction. More details can be found in [3].

To fully characterize the hysteresis in SCP actuators, the relationship between voltage input and the steady-state contraction length were measured under different loading forces. Loading forces were generated by attaching weights to the actuator, and the contraction length was measured based on the displacement of the weights. Since the time constants of the thermal dynamics are 1-5 s [4], each voltage step was held for 60 s, ensuring that the steady-state displacement would have been reached.

Fig. 2(a) shows a series of major hysteresis curves between voltage and displacement under loading forces ranging from 294 mN to 980 mN. The voltage range is [0, 5.1] V, and the displacement range is [0, 16.75] mm. Since the actuator length changes with loading forces, the initial displacement of each hysteresis curve is also different. Fig. 2(b) shows the relationships between displacement range and loading force, and between the initial displacement and loading force.

B. Why Hysteresis Modeling is Needed

In this paper, the term "index" refers to the numbering of the quasi-static voltage and displacement values. The performance is measured by the maximum and RMS percentages of the absolute errors divided by the displacement range:

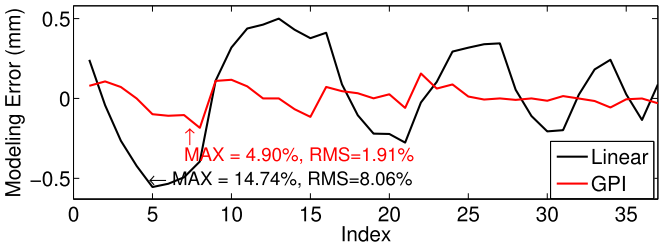

Fig. 3. Modeling error comparison between a GPI model and a linear model. The modeling performances of the models are shown in Fig. 1(d).

$$E_{\max} = \frac{\max_i\{|e_i|\}_{i=1}^{M}}{P} \times 100\%, \tag{1}$$

$$E_{\mathrm{RMS}} = \frac{\sqrt{\sum_{i=1}^{M}\{e_i^2\}_{i=1}^{M}/M}}{P} \times 100\%. \tag{2}$$

where e_i denotes the displacement error, M is the number of data-points to be evaluated, and P is the displacement range. They are denoted as the "maximum error" and the "RMS error" in this paper.

In order to better motivate this work, a GPI model and a linear model are compared for capturing the hysteresis when 30 g loading is used. Fig. 1(d) shows that the GPI model can accurately characterize the hysteresis, while the linear model can only provide a rough approximation. Fig. 3 shows the modeling errors of the two approaches. The effectiveness of the GPI model is evident. The GPI model will be described in depth in Section III. A Preisach model and a linear model will also be adopted in this work.

C. What's Unique About Coil-based Actuators

With the unique composition of twists and coils, the modeling and control of SCP actuators present unique challenges that do not lend themselves well to prior methods. Coiling and twisting of fiber threads was suggested to introduce friction and hysteretic nonlinear effects [1]. Although macro-scale helical spring analysis and molecular level chain interaction study can be adopted to study the physics of the SCP actuator [33], the analysis is complicated and does not consider hysteresis. This also means that SMA modeling is not directly applicable. SCP actuators modeling is an open challenge. Phenomenological hysteresis models provide a promising alternative for modeling the SCP actuators.

III. Proposed Hysteresis Models

In this section, an augmented hysteresis model is proposed by incorporating the relationship between hysteresis curves and loading forces. Three methods, namely, a GPI model, a Preisach model, and a linear model, are adopted to capture the hysteresis between normalized displacement and voltage.

A. Augmented Hysteresis Model

In order to characterize a series of hysteresis curves with different loading forces, individual hysteresis model could be separately identified and then combined [20]. However, then the model will be overly complicated. In [27], a Maxwell-slip model was proposed as a lumped-parametric model for pneumatic artificial muscle. The virgin curve equation was adopted to describe the friction force. Yet, because it only characterized a particular physical phenomenon (isotropic friction), the proposed method cannot be directly adopted.

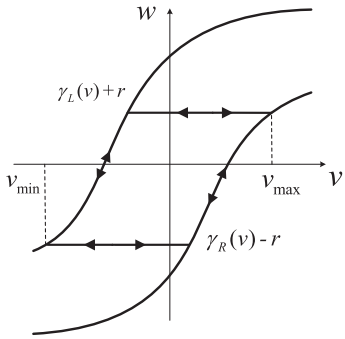

Fig. 4. A generalized play operator.

By modeling the relationship between the offset of hysteresis curve D and loading force F as $D = f_1(F)$, and the range of hysteresis curve P and loading force as $P = f_2(F)$, the following model is proposed:

$$y(t) = f_2(F) \cdot H[v](t) + f_1(F), \tag{3}$$

where $H[v](t)$ denotes the hysteresis between normalized displacement and voltage. Due to the fact that the hysteresis curves shown in Fig. 2(a) is monotonically decreasing, $H[v_{\min}](t) = 0$, $H[v_{\max}](t) = -1$. A GPI model, a Preisach model, and a linear model are employed to capture $H[v](t)$.

The proposed model assumes the relationship between displacement and loading force to be linear. In practice, hysteresis between displacement and force is observed, but relatively small (less than 7.5% error at most) whereas other hysteretic effects between voltage and displacement are significantly larger, and thus inverse compensation is performed on the dominant hysteresis variables. We will discuss our ideas on how one might define and handle multi-dimensional hysteresis (which is currently an open question in hysteresis modeling) in Section VII.

B. Augmented GPI Model

The GPI model consists of a weighted superposition of generalized play operators. For a given voltage input $v(t)$, the output $w(t)$ of a generalized play operator with radius r is written as (as shown in Fig. 4)

$$w(t) = G_r^{\gamma}[v](t) = g_r^{\gamma}(v(t), G_r^{\gamma}[v](t^-)), \tag{4}$$

where $g_r^{\gamma}(v(t), w(t^-))$ is defined as

$$g_r^{\gamma}(v(t), w(t^-)) = \begin{cases} \max(\gamma_R(v(t)) - r, w(t^-)), & \text{if } v(t) > v(t^-) \\ \min(\gamma_L(v(t)) + r, w(t^-)), & \text{if } v(t) < v(t^-) \\ w(t^-), & \text{if } v(t) = v(t^-), \end{cases} \tag{5}$$

where $t^- = \lim_{\epsilon>0,\epsilon\to 0} t-\epsilon$. The envelope functions of the generalized play operator, $\gamma_L(\cdot)$ and $\gamma_R(\cdot)$, are chosen to be strictly increasing. The condition $\gamma_R(v(t)) - r \le \gamma_L(v(t)) + r$ is required to meet the order preservation property of the hysteresis behavior [25].

The output of the GPI model is written in integral form:

$$y_e(t) = \int_0^R p(r) G_r^\gamma[v](t) dr + c, \tag{6}$$

where R is the maximum radius, $p(r)$ represents the weight function, and c is a constant bias.

In practical implementation, the integration is realized by discretization. The GPI model is adopted to fit $H[v](t)$ by

$$H_{\mathrm{GPI}}[v](t) = \sum_{j=0}^{N} p(r_j) G_{r_j}^\gamma[v](t) + c, \tag{7}$$

where $p(r_j)$ is the weight of the j-th generalized play operator, and r_j is the corresponding play radius. The number of the generalized play operators is $N+1$. This approach (Eq. (3) and Eq. (7)) is denoted as the "augmented GPI model".

Parameters of the GPI model can be identified through minimization of an error-squared function between the normalized experimental displacement and the model output. The minimization problem can be solved with the MATLAB command *fmincon*. More details can be found in [16]–[22].

C. Augmented Preisach Model

The Preisach model consists of a weighted superposition of delayed relays. Practical model implementation involves discretization of Preisach weight function to obtain a finite number of cells [24]. When the discretization level of the Preisach model is L, the number of cells is $L(L+1)/2$. The model parameter consists of the weight of each cell. The identification of the Preisach model can be reformulated as a constraint linear least-squares problem and solved with the MATLAB command *lsqnonneg*. More details can be found in [23]–[26]. The Preisach model is used to capture $H[v](t)$:

$$H_{\mathrm{Preisach}}[v](t) = \sum_{i=1}^{L} \sum_{j=1}^{L+1-i} \mu_{\mathrm{ij}} s_{\mathrm{ij}}[v](t) + c_2, \tag{8}$$

where μ_{ij} is the weight for cell (i,j), $s_{\mathrm{ij}}[v](t)$ is the signed area of the cell (i,j), which can be fully calculated based on voltage $v(t)$, c_2 is a constant bias. This approach (Eq. (3) and Eq. (8)) is denoted as the "augmented Preisach model".

D. Augmented Linear Model

Albeit simple, a linear model can be conveniently adopted:

$$H_{\mathrm{Linear}}[v](t) = kv(t) + c_3. \tag{9}$$

This approach (Eq. (3) and Eq. (9)) is denoted as the "augmented linear model". The identification of the linear model is solved with linear regression using MATLAB command *polyfit*. Since a linear term cannot capture the hysteresis behavior, it is expected that this approach would results in the worst modeling and control performance.

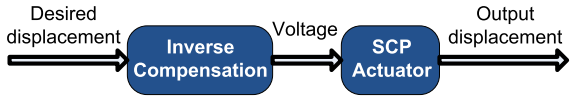

Fig. 5. Illustration of the inverse compensation of SCP actuators.

IV. Inverse Compensation

The goal of inverse compensation is to realize open-loop control by constructing an inverse hysteresis model to approximately cancel out the hysteresis, as shown in Fig. 5. The inverse of the augmented GPI model can be implemented efficiently, and the derivation is provided. The inverse of the other two approaches are also realized in this work, but the detailed derivation is not presented. The reader is referred to [17], [18], [22] for more details on GPI model inversion, and [23]–[26] on Preisach model inversion.

A. Inversion of GPI Model: $H_{\mathrm{GPI}}[v](t)$

Denote the desired output as y_d, the goal is to find $\hat{v}$, such that $y_d \approx H_{\mathrm{GPI}}[\hat{v}](t)$. The GPI model can be rewritten as [18]

$$\hat{v}(t) = \begin{cases} \gamma_R^{-1} \circ \Pi^{-1} \circ (y_d - c), & \text{if } y_d(t) > y_d(t^-) \\ \gamma_L^{-1} \circ \Pi^{-1} \circ (y_d - c), & \text{if } y_d(t) < y_d(t^-) \\ \hat{v}(t^-), & \text{if } y_d(t) = y_d(t^-), \end{cases} \tag{10}$$

where "$\circ$" denotes the composition of functions or operators, Π^{-1} is the inversion of a CPI model and is expressed as [17]

$$\Pi^{-1}[y_d - c](t) = \hat{p}(r_0)(y_d - c) + \sum_{k=1}^{N} \hat{p}(\hat{r}_k) F_{\hat{r}_k}[y_d - c](t), \tag{11}$$

where

$$\hat{r}_j = p(r_0) r_j + \sum_{k=1}^{j-1} p(r_k)(r_j - r_k), j \ge 1, \quad \hat{p}(r_0) = \frac{1}{p(r_0)},$$

and

$$\hat{p}(\hat{r}_k) = -\frac{p(r_k)}{(p(r_0) + \sum_{j=1}^{k} p(r_j))(p(r_0) + \sum_{j=1}^{k-1} p(r_j))}, \quad k = 1, \ldots, N.$$

B. Inversion of the Augmented GPI Model

Denote the desired output as y_d'. Rewrite Eq. (3) as

$$\sum_{j=0}^{N} p(r_j) H_{r_j}^\gamma[v](t) + c = \frac{y_d' - f_1(F)}{f_2(F)}. \tag{12}$$

The inverse of the augmented GPI model is expressed as

$$\hat{v}(t) = \begin{cases} \gamma_R^{-1} \circ \Pi^{-1} \circ (\frac{y_d' - f_1(F)}{f_2(F)} - c), & \text{if } y_d'(t) > y_d'(t^-), \\ \gamma_L^{-1} \circ \Pi^{-1} \circ (\frac{y_d' - f_1(F)}{f_2(F)} - c), & \text{if } y_d'(t) < y_d'(t^-), \\ \hat{v}(t^-), & \text{if } y_d'(t) = y_d'(t^-). \end{cases} \tag{13}$$

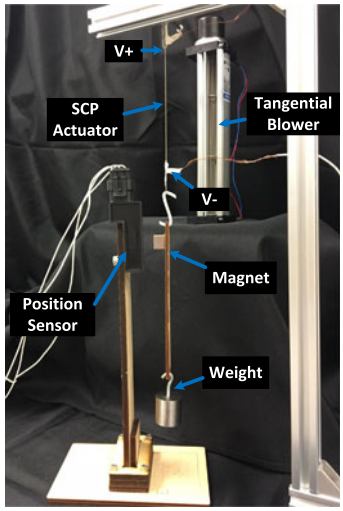

Fig. 6. The experimental setup for displacement and voltage measurements.

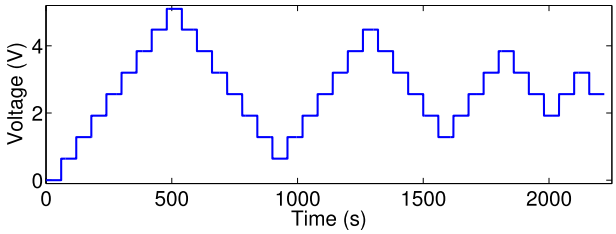

Fig. 7. The voltage input for model identification.

V. Experimental Setup

A. Material Selection and Manufacturing

While different materials can be utilized [4], we use the V Technical Textiles Conductive Yarns (110/34 dtex, Denier: 110/34f) to create SCP actuators. The off-the-shelf conductive nylon yarns are easily sourced in bulk quantities and still provide up to 8% strain. The proposed methods apply to SCP actuators with other composition methods [3].

The manufacturing process consists of coiling and heat treatment. The coiling can be realized as follows, one end of the thread is attached to a motor, and a weight (50 g) is hung on the other end to keep the thread taut. As the motor spins, the mass is not allowed to rotate, resulting in twists to the thread [4]. When the thread is completely coiled, it is double-backed to prevent unwinding. Fully coiled muscle is formed at 402 ± 10 rotations/cm (coiled and double backed length). The heat treatment procedure works by applying a square voltage pulse (1 sec on, 9 sec off) across the coiled thread, which heats the thread and then provides adequate cooling time. The peak voltage is chosen to be 1.0 V/cm of coiled thread length. After applying multiple voltage pulses, the length of the coiled thread converges and the muscle is obtained. The resting length of the SCP actuator used in this study was approximately 70 mm. More details on the manufacturing of SCP actuators can be found in [4].

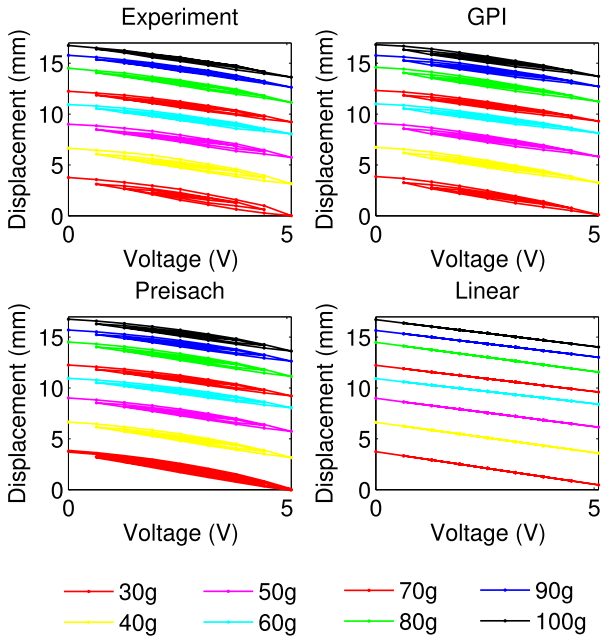

Fig. 8. The experimental hysteresis measurements between displacement and voltage under different loading forces, and modeling performances of the proposed three approaches.

B. Experimental Setup

The experimental testbed, as shown in Fig. 6, consists of an SCP actuator, a position sensor (SPS-L035-LATS, Honeywell) with 0.04 mm resolution, and a tangential blower fan (QG030-198/12, Ebm-papst) to provide even airflow environment, since pockets of hot air were otherwise spotted; refer to [4] on its effect to SCP actuation and relaxation. The position sensing mechanism is to measure the position of a magnet accurately by an array of magnetoresistive sensors. The additional mass of the magnet and components is about 20 g. Voltage steps were supplied by a pulse-width-modulated (PWM) circuit. Data acquisition was realized in Labview.

VI. Experimental Results

A. Model Identification

The voltage input is chosen to be in the form of damped oscillations, as shown in Fig. 7. Under a constant loading force, a single hysteresis curve between displacement and voltage can be obtained. A series of hysteresis curves are shown in Fig. 8 under different loading forces.

Although linear models can be adopted to approximate f_1 and f_2, the following 2^{nd}-order polynomials are utilized for increased accuracy, as shown in Fig. 2(b):

$$D = 8.685 \times 10^{-9} F^2 - 2.935 \times 10^{-5} F + 0.045, \quad (14)$$

$$P = -2.039 \times 10^{-9} F^2 + 5.527 \times 10^{-6} F - 0.005. \quad (15)$$

1) Augmented GPI Model: The number of the generalized play operators, $N+1$, is chosen to be 11. Further increasing $N+1$ does not produce appreciable improvement in modeling accuracy. In a similar way as [18], [19], [22], the radii are pre-defined as $r = (i-1)/10, i = 1, 2, \ldots, 11$. The envelope

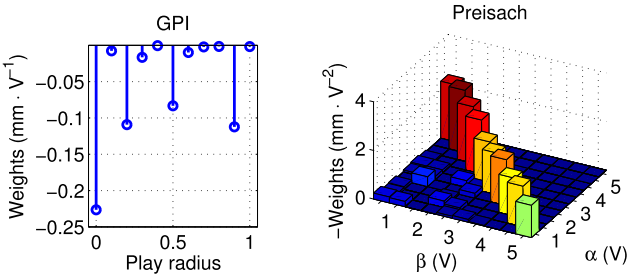

Fig. 9. Left figure: the identified weights, $p(r_j), j = 0, 1, \ldots, 10.$, of the augmented GPI model. Right figure: the identified weights of the augmented Preisach model.

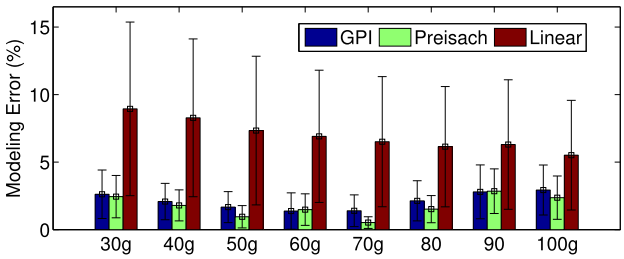

Fig. 10. The modeling error comparison of the proposed three models.

functions are chosen to be the following linear functions:

$$\gamma_R(v(t)) = a_R v(t) + b_R, \tag{16}$$

$$\gamma_L(v(t)) = a_L v(t) + b_L. \tag{17}$$

The parameters of the augmented GPI model are identified. Fig. 10 shows the weights of the proposed model. The weights are negative since the hysteresis is monotonically decreasing. It is identified that $a_R = 1.100$, $b_R = 0.048$, $a_L = 1.236$, $b_L = 0.088$, and $c = 0.396$. Figs. 8 and 10 show the modeling performance. Fig. 9 shows the modeling error and is obtained based on Fig. 8. According to Fig. 8, 37 different voltage steps are used in each loading condition and 8 loading conditions are tested, a total of 296 data points are adopted for the modeling error analysis. The maximum error and RMS error are 7.5% and 2.7%, respectively. This model can accurately capture the hysteresis of the SCP actuator.

2) Augmented Preisach Model: The number of discretization level of the model, L, is chosen to be 10. Fig. 9 shows the model weights. It is identified that $c_2 = 0.498$. Figs. 8 and 10 show the modeling performance. The maximum error and RMS error are 7.3% and 2.4%, respectively. While this model demonstrates comparable modeling accuracy as the augmented GPI model, the implementation is more complicated [22]. It is shown in Section VI.C that the inverse of this model is more computationally expensive than that of the augmented GPI model.

3) Augmented Linear Model: The augmented linear model is also realized. It is identified that $k = -0.173$, $c_3 = 0.008$. Figs. 8 and 10 show the modeling performance. The maximum error and RMS error are 20.4% and 6.9%, respectively. The augmented linear model can only provide a rough approximation of the hysteresis and results in the largest modeling error.

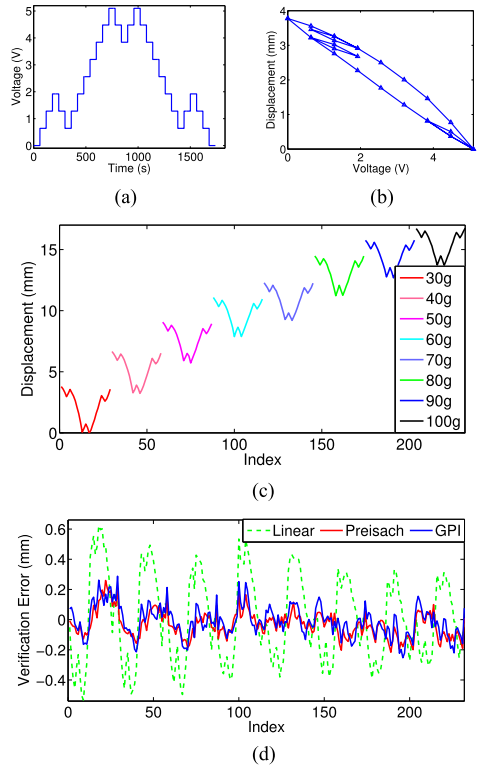

Methods	GPI	Preisach	Linear
Maximum error	8.8%	8.3%	19.8%
RMS error	3.2%	2.8%	7.7%

(e)

Fig. 11. (a) A voltage input for model verification. (b) The corresponding steady-state displacement trajectory under voltage input in (a) 30 g loading is used. (c) The corresponding experimental displacement measurements. (d) Errors in displacement predictions by the three modeling approaches. (e) The maximum error and RMS error comparison of the three models.

Overall, the augmented GPI model and the augmented Preisach model can effectively capture the hysteresis behavior in the SCP actuator. The RMS modeling errors are only around 3%. Considering that the existing linear methods have reported the modeling errors at 11% [12] and 7.8-9.3% [13], the proposed methods in this work is significantly better.

B. Model Verification

In order to further validate the effectiveness of the model, the model output and the experimental displacement can be compared under different loading conditions. Fig. 11(a) shows the voltage input that is applied to the SCP actuator, and Fig. 11(b) shows the corresponding steady-state displacement trajectory under 30 g loading. As can be seen, both the major hysteresis curve and minor hysteresis curves are traversed. The voltage input can indeed be utilized to verify the effectiveness of the proposed model. The experimental measurements of the steady-state displacement values are shown in Fig. 11(c), and each data point is obtained from a single trial under a particular loading condition. Since 29 different voltage steps are used in each loading condition and 8 loading conditions are tested, a total of 232 data points are obtained. Fig. 11(d) shows the

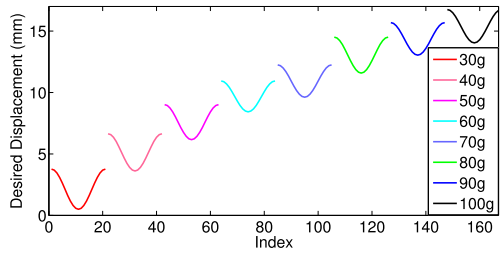

(a)

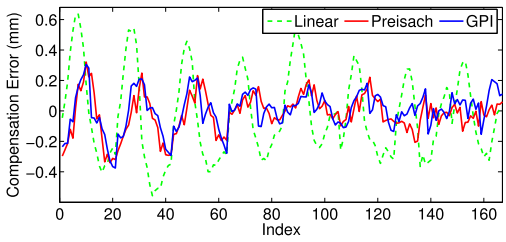

(b)

Methods	GPI	Preisach	Linear
Maximum error	11.7%	10.6%	20.2%
RMS error	4.0%	4.1%	8.9%

(c)

Fig. 12. (a) A series of desired sinusoidal reference displacements. (b) Inverse compensation errors of the proposed approaches. (c) The maximum and RMS tracking error comparison.

displacement estimation errors under each scheme. The corresponding maximum and RMS estimation errors are provided in Fig. 11(e). The augmented GPI model and the augmented Preisach model can accurately estimate the hysteresis of the SCP actuator.

C. Inverse Compensation

1) Displacement Control: The performance of the inverse compensation is examined in open-loop displacement tracking experiments. The desired displacement is chosen to be a series of sinusoidal profiles under different loading forces, as shown in Fig. 12(a), to test the effectiveness of the inverse compensation algorithms. Corresponding voltage step values are calculated off-line based on the inverse algorithms. Fig. 12(b) shows the compensation errors. The maximum and RMS tracking errors are provided in Fig. 12(c). It is shown that, the augmented GPI model-based compensation scheme outperforms the augmented linear model-based scheme in precision, and produces comparable performance as the augmented Preisach model-based compensation.

Note that the proposed control methods are all open-loop strategies, and it is understandable that the tracking errors are sightly higher than existing closed-loop control methods [4], [12], [13]. The advantages of the proposed open-loop inverse compensation method over the closed-loop strategies are that no displacement sensing equipment is needed and static motions can be realized. Furthermore, closed-loop control and inverse compensation can be adopted together for hysteretic systems [24], [31].

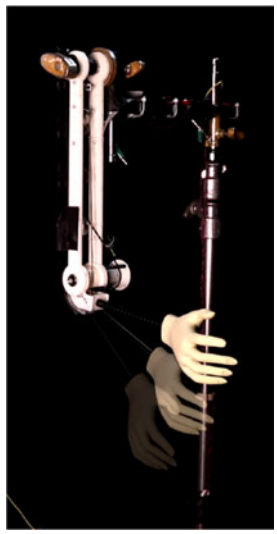

Fig. 13. A robotic arm actuated by three SCP actuators. The SCP actuators serve as bicep muscle to control the motion of the arm [4].

2) Computational Complexity: The inverse compensation in this work is quasi-static, since it considers the steady-state displacements. The compensation calculation is conducted off-line. The compensated system can be approximated as a linear system. Feedback control can be further developed, where the on-line inversion is required [24], [31]. The computational complexity of the inverse compensation is thus an important factor to consider.

The computational complexities of the augmented GPI model and Preisach model inverse are compared using the average time of each compensation calculation. The computations were run using Matlab on a Lenovo Thinkpad T420 with 2.80 GHz CPU and 4.00 GB memory. The average time for each calculation of the augmented GPI model inverse is 1.3 ms, while the average time for the augmented Preisach model inverse calculation is 5.4 ms. It is thus evident that the augmented GPI model is advantageous over the augmented Preisach model in overall accuracy and efficiency.

VII. Conclusion and Future Work

Three new hysteresis models are proposed to characterize the hysteresis between voltage input and contraction length of an SCP actuator. By incorporating the relationship between hysteresis curves and loading forces, the proposed models can efficiently estimate the hysteresis in SCP actuators under different loading forces. Open-loop position control is further realized through inverse compensation. Experimental results show that the proposed schemes can effectively estimate and compensate the hysteresis. The augmented GPI model presents the best overall performance considering its superior modeling and control accuracy and the good computational efficiency.

Being a widely-accessible and adaptable muscle-like actuator, the SCP actuators have the potential to transform artificial muscle technology, especially for robotic applications (e.g., robotic arm in Fig. 13). Their significant strain production could enable large range of robot motion, and their fast relaxation

property facilitates the realization of fast robot motion. Additional advantages include ease of manufacturing, low-cost, light-weight, and compliance.

The hysteresis model considered in this paper is quasi-static and rate-independent, since it describes the actuation behavior at the steady state under a series of constant voltage steps. In future work, the thermal dynamics of the SCP actuator will be incorporated, and closed-loop control will be investigated by combining feedback with the proposed inverse compensation scheme. In addition, for robotic applications such as the robotic arm in Fig. 13, the design challenge of identifying specific actuator configurations (size, range of actuation in load and in strain) can use the model developed in this paper to determine the optimal design of SCP actuators. An extension of this work is to perform multi-dimensional hysteresis characterization and inverse compensation, which would fully capture the minor system hystereses observed. As a higher order hysteresis model is proposed, the curse of dimensionality applies and the task of collecting sufficient experimental data to cover the hysteretic space becomes significant. Few strategies exist dealing with multi-variable hysteresis schemes, and none provide an inverse compensation method. Such methods will be useful for not only SCP actuators but also SMAs and other artificial muscles, and is worth investigating.

REFERENCES

[1] J. D. W. Madden and S. Kianzad, "Twisted lines: Artificial muscle and advanced instruments can be formed from nylon threads and fabric," *IEEE Pulse*, vol. 6, no. 1, pp. 32–35, Jan./Feb. 2015.

[2] M. D. Lima *et al.*, "Electrically, chemically, and photonically powered torsional and tensile actuation of hybrid carbon nanotube yarn muscles," *Science*, vol. 338, no. 6109, pp. 928–932, 2012.

[3] C. S. Haines *et al.*, "Artificial muscles from fishing line and sewing thread," *Science*, vol. 343, no. 6173, pp. 868–872, 2014.

[4] M. Yip and G. Niemeyer, "High-performance robotic muscles from conductive nylon sewing thread," in *Proc. IEEE Int. Conf. Robot.and Autom.*, 2015, pp. 2313–2318.

[5] J. M. Jani, M. Leary, A. Subic, and M. A. Gibson, "A review of shape memory alloy research, applications and opportunities," *Mater. Design*, vol. 56, pp. 1078–1113, 2014.

[6] R. Romano and E. A. Tannuri, "Modeling, control and experimental validation of a novel actuator based on shape memory alloys," *Mechatronics*, vol. 19, no. 7, pp. 1169–1177, 2009.

[7] S. M. Mirvakili *et al.*, "Simple and strong: Twisted silver painted nylon artificial muscle actuated by joule heating," *Proc. SPIE*, vol. 9056, 2014, Art. no. 90560I.

[8] S. K. Kianzad *et al.*, "Nylon coil actuator operating temperature range and stiffness," *Proc. SPIE*, vol. 9430, 2015, Art. no. 94301X.

[9] S. Kianzad, J. D. Pandit, Milind Lewis, A. R. Berlingeri, K. J. Haebler, and J. D. Madden, "Variable stiffness and recruitment using nylon actuators arranged in a pennate configuration," *Proc. SPIE*, vol. 9430, 2015, Art. no. 94301Z.

[10] K. H. Cho *et al.*, "A robotic finger driven by twisted and coiled polymer actuator," *Proc. SPIE*, vol. 9798, 2016, Art. no. 97981J.

[11] L. Wu *et al.*, "Nylon-muscle-actuated robotic finger," *Proc. SPIE*, vol. 9431, 2015, Art. no. 94310I.

[12] L. Sutton, H. Moein, A. Rafiee, J. D. W. Madden, and C. Menon, "Design of an assistive wrist orthosis using conductive nylon actuators," in *Proc. IEEE Int. Conf. Biomed. Robot. Biomechatronics*, 2016, pp. 1074–1079.

[13] T. Arakawa, K. Takagi, K. Tahara, and K. Asaka, "Position control of fishing line artificial muscles (coiled polymer actuators) from nylon thread," *Proc. SPIE*, vol. 9798, 2016, Art. no. 97982W.

[14] Y. Li and Z. Wu, "Stabilization of floating offshore wind turbines by artificial muscle based active mooring line force control," in *Proc. Amer. Control Conf.*, 2016, pp. 2277–2282.

[15] D. Jiles and D. Atherton, "Theory of ferromagnetic hysteresis," *J. Magn. Magn. Mater.*, vol. 61, no. 1, pp. 48–60, 1986.

[16] O. Al Janaideh, M. Al Janaideh, and M. Rakotondrabe, "Inversion-free feedforward dynamic compensation of hysteresis nonlinearities in smart micro/nano-positioning actuator," in *Proc. IEEE Int. Conf. Robot. Autom.*, 2015, pp. 2673–2678.

[17] P. Krejci and K. Kuhnen, "Inverse control of systems with hysteresis and creep," *IEE P-Contr. Theory Appl.*, vol. 148, no. 3, pp. 185–192, 2001.

[18] M. Al Janaideh, S. Rakheja, and C.-Y. Su, "An analytical generalized Prandtl-Ishlinskii model inversion for hysteresis compensation in micropositioning control," *IEEE/ASME Trans. Mech.*, vol. 16, no. 4, pp. 734–744, Aug. 2011.

[19] J. Zhang, E. Merced, N. Sepúlveda, and X. Tan, "Modeling and inverse compensation of hysteresis in vanadium dioxide using an extended generalized Prandtl-Ishlinskii model," *Smart Mater. Struct.*, vol. 23, no. 12, 2014, Art. no. 125017.

[20] Z. Zhang, Q. W. Chen, J. Mao, and Z. Wang, "A generalized stress-dependent Prandtl-Ishlinskii model and its adaptive inverse compensation with model reference for GMA," in *Proc. Asian Control Conf.*, 2011, pp. 535–540.

[21] Z. Sun, B. Song, N. Xi, R. Yang, L. Hao, and L. Chen, "Compensating asymmetric hysteresis for nanorobot motion control," in *Proc. IEEE Int. Conf. Robot. Autom.*, 2015, pp. 3501–3506.

[22] J. Zhang, D. Torres, J. Ebel, N. Sepúlveda, and X. Tan, "A composite hysteresis model in self-sensing feedback control of fully integrated VO_2 microactuators," *IEEE/ASME Trans. Mech.*, vol. 21, no. 5, pp. 2405–2417, Oct. 2016.

[23] K. K. Leang, Q. Zou, and S. Devasia, "Feedforward control of piezoactuators in atomic force microscope systems," *IEEE Control Syst.*, vol. 29, no. 1, pp. 70–82, Feb. 2009.

[24] X. Tan and J. Baras, "Modeling and control of hysteresis in magnetostrictive actuators," *Automatica*, vol. 40, no. 9, pp. 1469–1480, 2004.

[25] R. Iyer and X. Tan, "Control of hysteretic systems through inverse compensation," *IEEE Control Syst. Mag.*, vol. 29, no. 1, pp. 83–99, Feb. 2009.

[26] S. Shao, M. Xu, S. Zhang, and S. Xie, "Stroke maximizing and high efficient hysteresis hybrid modeling for a rhombic piezoelectric actuator," *Mech. Syst. Signal Process.*, vol. 75, pp. 631–647, 2016.

[27] T. Vo-Minh, T. Tjahjowidodo, H. Ramon, and H. V. Brussel, "A new approach to modeling hysteresis in a pneumatic artificial muscle using the maxwell-slip model," *IEEE/ASME Trans. Mech.*, vol. 16, no. 1, pp. 177–186, Feb. 2011.

[28] Q. P. Ha, S. Royel, J. Li, and Y. Li, "Hysteresis modeling of smart structure MR devices using describing functions," *IEEE/ASME Trans. Mech.*, vol. 21, no. 1, pp. 44–50, Feb. 2016.

[29] D. Habineza, M. Rakotondrabe, and Y. Le Gorrec, "Bouc-Wen modeling and feedforward control of multivariable hysteresis in piezoelectric systems: Application to a 3-DoF piezotube scanner," *IEEE Trans. Control Syst. Technol.*, vol. 23, no. 5, pp. 1797–1806, Sep. 2015.

[30] L. Shu, G. Wu, D. Chen, and M. J. Dapino, "Modeling of galfenol bending actuator considering nonlinear hysteresis and dynamic real-time control strategy," *Smart Mater. Struct.*, vol. 25, no. 3, p. 035046, 2016.

[31] S. Devasia, E. Eleftheriou, and S. O. R. Moheimani, "A survey of control issues in nanopositioning," *IEEE Tran. Control Syst. Technol.*, vol. 15, no. 5, pp. 802–823, Sep. 2007.

[32] J. Yi, S. Chang, and Y. Shen, "Disturbance-observer-based hysteresis compensation for piezoelectric actuators," *IEEE/ASME Trans. Mech.*, vol. 14, no. 4, pp. 456–464, Aug. 2009.

[33] Q. Yang and G. Li, "A top-down multi-scale modeling for actuation response of polymeric artificial muscles," *J. Mech. Phys. Solids*, vol. 92, pp. 237–259, 2016.